

A simple model for semipermeable membrane: Donnan equilibrium

Felipe Jiménez-Ángeles* and Marcelo Lozada-Cassou†

Programa de Ingeniería Molecular, Instituto Mexicano del Petróleo,

Lázaro Cárdenas 152, 07730 México, D. F., México and

Departamento de Física, Universidad Autónoma Metropolitana-Iztapalapa, Apartado Postal 55-334, 09340 D.F. México

We study a model for macroions in an electrolyte solution confined by a semipermeable membrane. The membrane finite thickness is considered and both membrane surfaces are uniformly charged. The model explicitly includes electrostatic and size particles correlations. Our study is focused on the adsorption of macroions on the membrane surface and on the osmotic pressure. The theoretical prediction for the osmotic pressure shows a good agreement with experimental results.

Keywords: Donnan equilibrium, semipermeable membrane, charge reversal, charge inversion, adsorption, macroions.

PACS numbers:

I. INTRODUCTION

Physics of two ionic solutions separated by a semipermeable membrane is of wide interest in cell biology and colloids science [1, 2, 3]. A thermodynamical study of this problem was first carried out by F. G. Donnan [4, 5], considering the two fluids phases (here referred as α and β) in the following way: (i) the α -phase contains two (small) ionic species, (ii) the β -phase contains the same ionic species as the α -phase plus one macroion species. The two fluid phases are separated by a membrane which is permeable to the small ions and impermeable to macroions, therefore, they interchange small ions whereas macroions are restricted to the β -phase. The permeability condition is imposed by assuming (in both phases) a constant chemical potential of the permeating species. In this simple model, Donnan derived an expression for the osmotic pressure (in terms of the ionic charge, concentration and excluded volume) which well describes systems close to ideality. Historically, this problem has been known as Donnan equilibrium. More recently some theories have been proposed to interpret osmotic pressure data [6, 7]. These theories consider phenomenologically the macroion-macroion and ion-macroion many-body interactions, and provide a better fit for the osmotic pressure of macroions solutions than Donnan theory.

The surface of a biological membrane has a net charge when it is in aqueous solution [1] thus, at a fluid-membrane interface a broad variety of phenomena occur. It is known that ionic solutions in the neighborhood of a charged surface produce an exponentially decaying charge distribution, known as the electrical double layer. Low-concentrated solutions of monovalent ions are well described by the Gouy-Chapman theory (Poisson-Boltzmann equation) [8, 9]. However, multivalent ions display important deviations from this picture [10] and more powerful theories from modern statisti-

cal mechanics (such as molecular simulation [11, 12, 13], density functionals [14, 15, 16] and integral equations [17, 18, 19, 20, 21]) have been implemented for studying ions adsorption and interfacial phenomena. Macroions adsorption is a subject of current interest: In molecular engineering, the macroions adsorption mechanisms are basic in self-assembling polyelectrolyte layers on a charged substrate [22] and novel colloids stabilization mechanisms [23].

By means of integral equations, a previous study of Donnan equilibrium has been carried out by Zhou and Stell [24, 25]. They used the method proposed by Henderson *et al.* [17], which can be described as follows: starting from a semipermeable spherical cavity [26], the planar membrane is obtained taking the limit of infinite cavity radius. Within this model, they obtained the charge distribution and mean electrostatic potential. However, due to the approximations used, they end up just with the integral version of the linear Poisson-Boltzmann equation. A general shortcoming of the Poisson-Boltzmann equation is that ionic size effects (short range correlations) are completely neglected, in consequence, the description of interfacial phenomena and computation of thermodynamical properties is limited and valid only for low values of charge and concentration.

From previous studies of two fluid phases separated by a *permeable* membrane, it is known that the adsorption phenomena are strongly influenced by the membrane thickness [27, 28, 29]. On the other hand, short range correlations influence effective colloid-colloid interaction [30, 31, 32, 33, 34], thermodynamical properties [35] and adsorption phenomena [36, 37] in colloidal dispersions. From these antecedents it is seen that there are several relevant aspects not considered in previous studies of Donnan equilibrium which deserve a proper consideration. In this study we consider explicitly the following effects: many-body (short and long range) correlations, the membrane thickness and the surface charge densities on each of the membrane faces. We use *simple* model interactions and our study is carried out by means of integral equations. The theory gives the parti-

*Electronic address: fangeles@imp.mx

†Electronic address: marcelo@imp.mx

cles distribution in the neighborhood of the membrane, from which, the osmotic pressure is calculated. There are two points that we will address in this study: the adsorption of macroions at the membrane surface and the computation of the osmotic pressure for macroions solutions. Concerning the adsorption phenomena, we observe a broad variety of phenomena: charge reversal, charge inversion and macroions adsorption on a like-charged surface due to the fluid-fluid correlation. The computed osmotic pressure is compared with experimental results for a protein solution, obtaining an excellent agreement over a wide regime of concentrations.

The paper is organized as follows: In section II we describe the integral equations method and the membrane and fluid models. In the same section, we derive the *hypernetted chain/mean spherical* (HNC/MS) integral equations for the semipermeable membrane and the equations to compute the osmotic pressure. In section III a variety of results are discussed and finally in section IV some conclusions are presented.

II. THEORY

A. Integral equations for inhomogeneous fluids

The method that we use to derive integral equations for inhomogeneous fluids makes use of a simple fact: In a fluid, an external field can be considered as a particle in the fluid, i. e., as one more species infinitely dilute. This statement is valid in general, however, it is particularly useful in the statistical mechanics theory for inhomogeneous fluids [18, 38] described below.

The multi-component Ornstein-Zernike equation for a fluid made up of $n + 1$ species is

$$h_{ij}(\mathbf{r}_{21}) = c_{ij}(\mathbf{r}_{21}) + \sum_{m=1}^{n+1} \rho_m \int h_{im}(\mathbf{r}_{23}) c_{mj}(\mathbf{r}_{13}) dv_3, \quad (1)$$

where ρ_m is the number density of species m , $h_{ij}(\mathbf{r}_{21}) \equiv g_{ij}(\mathbf{r}_{21}) - 1$ and $c_{ij}(\mathbf{r}_{21})$ are the total and direct correlation functions for two particles at \mathbf{r}_2 and \mathbf{r}_1 of species i and j , respectively; with $g_{ij}(\mathbf{r}_{21})$ the pair distribution and $\mathbf{r}_{21} = \mathbf{r}_2 - \mathbf{r}_1$. Among the most known closures between $h_{ij}(\mathbf{r}_{21})$ and $c_{ij}(\mathbf{r}_{21})$ used to solve Eq. (1), we have [39]

$$c_{ij}(\mathbf{r}_{21}) = -\beta u_{ij}(\mathbf{r}_{21}) + h_{ij}(\mathbf{r}_{21}) - \ln g_{ij}(\mathbf{r}_{21}), \quad (2)$$

$$c_{ij}(\mathbf{r}_{21}) = f_{ij}(\mathbf{r}_{21}) \exp\{-\beta u_{ij}(\mathbf{r}_{21})\} g_{ij}(\mathbf{r}_{21}), \quad (3)$$

$$c_{ij}(\mathbf{r}_{21}) = -\beta u_{ij}(\mathbf{r}_{21}) \text{ for } r_{21} \equiv |\mathbf{r}_{21}| \geq a_{ij}. \quad (4)$$

Eqs. (2) to (4) are known as the hypernetted chain (HNC), the Percus-Yevick (PY) and the mean spherical (MS) approximations, respectively; $u_{ij}(\mathbf{r}_{21})$ is the direct interaction potential between two particles of species i and j , a_{ij} is their closest approach distance, $f_{ij}(\mathbf{r}_{21}) \equiv$

$\exp\{-\beta u_{ij}(\mathbf{r}_{21})\} - 1$, and $\beta \equiv 1/k_B T$. Some more possibilities to solve Eq. (1) are originated by considering a closure for $c_{ij}(\mathbf{r}_{21})$ in the first term of Eq. (1) and a different one for $c_{mj}(\mathbf{r}_{13})$ in the second term of Eq. (1), giving rise to hybrid closures.

To derive integral equations for inhomogeneous fluids, we let an external field to be one of the fluid species, say $(n + 1)$ -species (denoted as the γ -species), which is required to be infinitely dilute, i. e., $\rho_\gamma \rightarrow 0$. Therefore, the total correlation function between a γ -species particle and a j -species particle is given by

$$h_{\gamma j}(\mathbf{r}_{21}) = c_{\gamma j}(\mathbf{r}_{21}) + \sum_{m=1}^n \rho_m \int h_{\gamma m}(\mathbf{r}_{23}) c_{mj}(\mathbf{r}_{13}) dv_3 \quad \text{with } j = 1, \dots, n. \quad (5)$$

The total correlation functions for the remaining species satisfy a n -component Ornstein-Zernike equation as Eq. (1) (with no γ species) from which $c_{mj}(\mathbf{r}_{13})$ is obtained. In this scheme, the pair correlation functions, $g_{\gamma i}(\mathbf{r}_{21})$, is just the inhomogeneous one-particle distribution function, $g_i(\mathbf{r}_1)$, for particles of species j under the influence of an external field. Thus, $h_{\gamma j}(\mathbf{r}_{21})$ and $c_{\gamma j}(\mathbf{r}_{21})$ can be replaced with $h_j(\mathbf{r}_1) \equiv g_j(\mathbf{r}_1) - 1$ and $c_j(\mathbf{r}_1)$, respectively. Thus, the inhomogeneous local concentration for the j species is given by

$$\rho_j(\mathbf{r}_1) = \rho_j g_j(\mathbf{r}_1), \quad (6)$$

By using the HNC closure (Eq. (7)) for $c_{\gamma j}(\mathbf{r}_{21})$ in Eq. (5), we get

$$g_j(\mathbf{r}_1) = \exp \left\{ -\beta u_j(\mathbf{r}_1) + \sum_{m=1}^n \rho_m \int h_m(\mathbf{r}_3) c_{mj}(\mathbf{r}_{13}) dv_3 \right\}, \quad (7)$$

where the subindex γ has been omitted for consistency with Eq. (6). In our approach, $c_{mj}(\mathbf{r}_{13})$ in the integral of Eq. (7), is approximated by the direct correlation function for a n -component homogeneous fluid. Thus, $c_{mj}(\mathbf{r}_{13})$ is obtained from Eq. (1) using one of the closures provided by Eqs. (2)-(4). For the present derivation we will use $c_{mj}(\mathbf{r}_{13})$ obtained with the MS closure (Eq. (4)), therefore, we obtain the hypernetted chain/mean spherical (HNC/MS) integral equations for an inhomogeneous fluid. This equation has shown to be particularly successful in the case of inhomogeneous charged fluids when it is compared with molecular simulation data [40, 41, 42, 43].

B. The semipermeable membrane and fluid models

The membrane is modelled as a planar hard wall of thickness d , and charge densities σ_1 and σ_2 on each surface and separates two fluid phases, referred as α and β . In Fig. 1, σ_1 and the α -phase are at the left hand side, whereas σ_2 and the β -phase are at the right hand side. The fluid phased are made up in the following way:

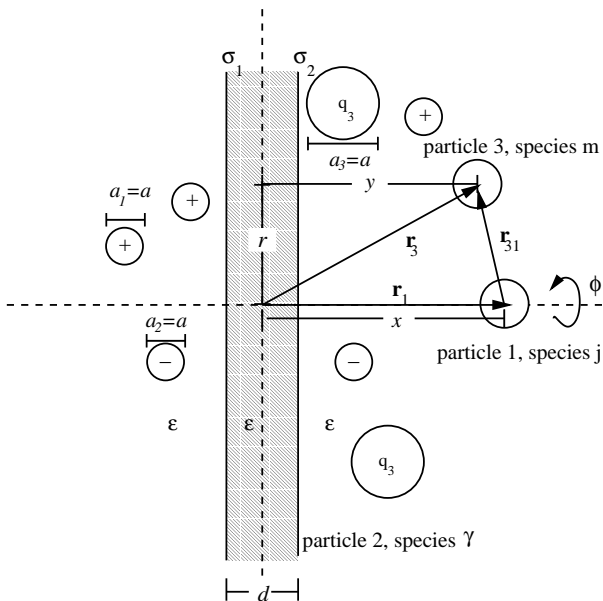


FIG. 1: Schematic representation for a model macroions solution confined by a semipermeable membrane. For the integration of Eq. (18) it is considered the *axial* symmetry around the \mathbf{r}_1 vector where we fix a cylindrical coordinates system (ϕ, r, y) .

(i) The α -phase is a two component electrolyte, considering the components to be hard spheres of diameter a_i with a centered point charge $q_i = z_i e$ (being z_i and e the ionic valence and the proton's charge, respectively) and $i = 1, 2$ standing for the species number. The solvent is considered as a uniform medium of dielectric constant ε . (ii) The β -phase is considered in the same way as the α -phase (same solvent dielectric constant and containing the same ionic species) plus one more species (species 3) of diameter a_3 and charge q_3 . For simplicity, we have considered that the membrane dielectric constant is equal to that of the solvent. In addition it is considered that

$$\begin{aligned} a &\equiv a_1 = a_2 \leq a_3, \\ z &\equiv z_1 = -z_2. \end{aligned} \quad (8)$$

Hence, we refer to the third species as the macroion species. Two ions of species m and j with relative position r , interact via the following potential

$$u_{mj}(r) = \begin{cases} \infty & \text{for } r < a_{mj}, \\ \frac{z_m z_j e^2}{\varepsilon r} & \text{for } r \geq a_{mj}, \end{cases} \quad (9)$$

with $m, j = 1, \dots, 3$ and $a_{mj} \equiv \frac{a_m + a_j}{2}$. Far away from the membrane each phase is homogeneous and neutral, thus the neutrality condition is written as

$$\sum_{i=1}^2 z_i \rho_i^\alpha = \sum_{i=1}^3 z_i \rho_i^\beta = 0, \quad (10)$$

being ρ_i^α and ρ_i^β the bulk concentrations of the i species in the α and β phases, respectively. The charge on the membrane is compensated by an excess of charge in the fluid (per unit area), σ' [44, 45]:

$$\sigma' \equiv \sigma^\alpha + \sigma^\beta = -\sigma_T, \quad (11)$$

with $\sigma_T = \sigma_1 + \sigma_2$ and being σ^α and σ^β the excess of charge in the α -phase and β -phase, respectively, which are given by

$$\sigma^\alpha = \int_{-\infty}^{-\frac{d}{2}} \rho_{el}(x) dx \quad (12)$$

and

$$\sigma^\beta = \int_{\frac{d}{2}}^{\infty} \rho_{el}(x) dx, \quad (13)$$

being

$$\rho_{el}(x) \equiv e \sum_{m=1}^3 z_m \rho_m(x), \quad (14)$$

the local charge density profile. In Eqs. (12), (13) and (14) it has been considered that the particles reduced concentration profile ($g_j(\mathbf{r}_1)$) depends only on the perpendicular position to the membrane, x , i. e., $g_j(\mathbf{r}_1) = g_j(x)$. Hence, the local concentration profile is $\rho_m(x) = \rho_m g_m(x)$.

According to the integral equations method outlined in section II A, the membrane is considered as the fluid species labelled as species γ (see Fig. 1). The interaction potential between the membrane and a j -species particle depends only on the particle position, x , referred to a coordinates system set in the middle of the membrane and measured perpendicularly. Thus, we write $u_j(\mathbf{r}_1) = u_j(x)$ which is split as $u_j(x) = u_j^{el}(x) + u_j^*(x)$, being $u_j^{el}(x)$ the direct electrostatic potential and $u_j^*(x)$ the hard-core interaction. The former can be found from Gauss' law, resulting

$$-\beta u_j^{el}(x) = \begin{cases} \frac{2\pi}{\varepsilon} z_j e \beta \sigma_T (x - L) & \text{for } x \geq \frac{d}{2}, \\ \frac{2\pi}{\varepsilon} z_j e \beta [\sigma_T (-x - L) - (\sigma_1 - \sigma_2) d] & \text{for } x \leq \frac{-d}{2}, \end{cases} \quad (15)$$

where L is the location of a reference point. The hard-core interaction is given by

$$u_j^*(x) = \begin{cases} \infty & \text{for } |x| < \frac{d+a}{2}, \\ 0 & \text{for } |x| \geq \frac{d+a}{2}, \end{cases} \quad (16)$$

for $j = 1, 2$. For the impermeable species ($j = 3$)

$$u_3^*(x) = \begin{cases} \infty & \text{for } x < \frac{d+a_3}{2}, \\ 0 & \text{for } x \geq \frac{d+a_3}{2}. \end{cases} \quad (17)$$

This potential imposes $g_3(x) = 0$ for $x \leq \frac{d+a_3}{2}$.

In Eq. (7) we use the expression of $c_{mj}(r_{13})$ for a primitive model *bulk* electrolyte, which has an analytical expression, written as

$$c_{mj}(r_{13}) = \begin{cases} -\beta u_{mj}^{el}(r_{13}) = -\beta \frac{z_m z_j e^2}{\epsilon r} & \text{for } r_{13} \geq a_{mj}, \\ c_{mj}^{sr}(r_{13}) + c_{mj}^{hs}(r_{13}) & \text{for } r_{13} < a_{mj}, \end{cases} \quad (18)$$

where $r_{13} \equiv |\mathbf{r}_{13}|$ is the relative distance between two ions of species m and j . The particles short range correlations are considered through the $c_{mj}^{sr}(r_{13})$ and $c_{mj}^{hs}(r_{13})$. The explicit form of these functions is given in appendix A. The integral in Eq. (7) can be expressed in cylindrical coordinates, and analytically calculated in the ϕ and r variables (see Fig. 1), i. e., we consider a cylindrical coordinates system where $r_{13}^2 = x^2 + r^2 + y^2 - 2xy$ and $dv_3 = d\phi r dr dy$. After a lengthy algebra, from Eq. (7) we get [44, 45]

$$\begin{aligned} g_j(x) = & \exp \left\{ \frac{2\pi}{\epsilon} z_j e \beta (\sigma_1 + \sigma_2) |x| - 2\pi A_j(x) \right. \\ & + 2\pi \sum_{m=1}^2 \rho_m \int_{-\infty}^{-\frac{d+a_m}{2}} h_m(y) G_{mj}(x, y) dy \\ & + 2\pi \sum_{m=1}^3 \rho_m \int_{\frac{d+a_m}{2}}^{\infty} h_m(y) G_{mj}(x, y) dy \\ & + 2\pi z_j \frac{e^2 \beta}{\epsilon} \sum_{m=1}^2 z_m \rho_m \int_{-\infty}^{-\frac{d+a_j}{2}} g_m(y) [y + |x - y|] dy \\ & \left. + 2\pi z_j \frac{e^2 \beta}{\epsilon} \sum_{m=1}^3 z_m \rho_m \int_{\frac{d+a_m}{2}}^{\infty} h_m(y) [y + |x - y|] dy \right\}. \end{aligned} \quad (19)$$

The first and third integrals include $h_j(y) = g_j(y) - 1$ for particles in the α -phase whereas, the second and fourth integrals, for particles in the β -phase. Notice the different summation limits due to the different phase composition. We have defined

$$G_{mj}(x, y) = L_{mj}(x, y) + K_{mj}(x, y), \quad (20)$$

$$L_{mj}(x, y) = \int_{|x-y|}^{\infty} c_{mj}^{sr}(r_{13}) r_{13} dr_{13} = \frac{e^2 \beta}{\epsilon} D_{mj}(x, y), \quad (21)$$

$$K_{mj}(x, y) = \int_{|x-y|}^{\infty} c_{mj}^{hs}(r_{13}) r_{13} dr_{13}, \quad (22)$$

and

$$\begin{aligned} A_j(x) = & \rho_3 \int_{-\infty}^{\frac{d+a_3}{2}} G_{3j}(x, y) dy \\ & + \sum_{m=1}^2 \rho_j \int_{-\frac{d+a_m}{2}}^{\frac{d+a_m}{2}} G_{mj}(x, y) dy \\ & + z_j z_3 \rho_3 \frac{\beta e^2}{\epsilon} \int_{\frac{d+a_3}{2}}^{\frac{d+a_3}{2}} [y + |x - y|] dy \\ & + z_j e \frac{\beta d}{\epsilon} (\sigma_1 - \sigma_2) \Theta(x + d/2), \end{aligned} \quad (23)$$

with $\Theta(x)$ the step function, defined as

$$\Theta(x) = \begin{cases} 0 & \text{for } x < 0, \\ 1 & \text{for } x \geq 0. \end{cases} \quad (24)$$

The expressions for the kernels, $K_{mj}(x, y)$ and $D_{mj}(x, y)$, are given in appendix A.

From the solution of Eq. (19) one obtains the reduced concentration profile, $\rho_j(x) = \rho_j g_j(x)$. The *bulk* concentrations of species j , at the α and β phases (ρ_j^α and ρ_j^β) are given by

$$\rho_j^\beta = \lim_{x \rightarrow \infty} \rho_j g_j(x), \quad (25)$$

and

$$\rho_j^\alpha = \lim_{x \rightarrow -\infty} \rho_j g_j(x), \quad (26)$$

respectively. At the β phase $g_j(x) \rightarrow 1$ as $x \rightarrow \infty$ then $\rho_j^\beta = \rho_j$. On the other hand, in the α phase (for $x < 0$), $\lim_{x \rightarrow -\infty} g_j(x) \neq 1$. It must be pointed out that the electrolyte bulk concentration at the α -phase (ρ_j^α , for $j = 1, 2$) satisfy the bulk electroneutrality condition, Eq. (10), and are a result from the theory.

C. Computation of the osmotic pressure: contact theorem

Let us consider a slice of fluid of width dx , area of its faces, A , parallel to the membrane and located at x . The force on the slice in the x direction, dF_x , is given by [46]

$$dF_x(x) = E_x(x) dQ + S dp(x) \quad (27)$$

being $E_x(x)$ the electric field in the x direction at x , dQ the total charge in the fluid slice and $dp(x)$ the pressure difference at the two faces. Taking into account that

$$E_x(x) = -\frac{\partial \psi(x)}{\partial x}, \quad (28)$$

and using Poisson's equation,

$$\frac{\partial^2 \psi(x)}{\partial x^2} = -\frac{4\pi}{\epsilon} \rho_{el}(x), \quad (29)$$

we write

$$dQ = A\rho_{el}(x)dx = -\frac{A\varepsilon}{4\pi} \left(\frac{\partial^2 \psi(x)}{\partial x^2} \right) dx. \quad (30)$$

Thus, we rewrite Eq. (27) as

$$dF_x(x) = \frac{A\varepsilon}{4\pi} \left(\frac{\partial \psi(x)}{\partial x} \right) \left(\frac{\partial^2 \psi(x)}{\partial x^2} \right) dx + Adp(x), \quad (31)$$

or equivalently,

$$dF_x(x) = \frac{A\varepsilon}{8\pi} \frac{\partial}{\partial x} \left(\frac{\partial \psi(x)}{\partial x} \right)^2 dx + Adp(x). \quad (32)$$

Considering that in equilibrium $dF_x(x) = 0$ and integrating Eq. (32) in the interval $[d/2, \infty)$ with the boundary condition

$$\lim_{x \rightarrow \infty} \frac{\partial \psi(x)}{\partial x} = 0, \quad (33)$$

we obtain

$$\frac{\varepsilon}{8\pi} \left(\frac{\partial \psi(x)}{\partial x} \right)_{x=x_0}^2 + (p_0^\beta - \Pi^\beta) = 0, \quad (34)$$

where $\Pi^\beta \equiv \lim_{x \rightarrow \infty} p(x)$ is the bulk fluid pressure and the expression for the pressure on the membrane right surface, $p_0^\beta \equiv p(0)$, is given by

$$p_0^\beta = k_B T \rho_T^\beta(0) = k_B T \sum_{i=1}^3 \rho_i g_i \left(\frac{d+a_i}{2} \right), \quad (35)$$

where $\rho_T^\beta(0) = \sum_{i=1}^3 \rho_i \left(\frac{d+a_i}{2} \right)$. Eq. (35) is an *exact* relationship which can be obtained by considering the force on the fluid (at the contact plane) exerted by the *hard* wall [47]. From basic electrostatics we have

$$\frac{\varepsilon}{4\pi} \left(\frac{\partial \psi(x)}{\partial x} \right)_{x=d/2} = \int_{d/2}^{\infty} \rho_{el}(x) dx, \quad (36)$$

thus, using Eqs. (34), (35) and (36) we can write

$$\Pi^\beta = \frac{2\pi}{\varepsilon} \left[\int_{d/2}^{\infty} \rho_{el}(x) dx \right]^2 + k_B T \sum_{i=1}^3 \rho_i g_i \left(\frac{d+a_i}{2} \right), \quad (37)$$

where the first term can be identified as the Maxwell stress tensor. A similar expression is obtained for the bulk pressure in the α phase

$$\Pi^\alpha = \frac{2\pi}{\varepsilon} \left[\int_{-\infty}^{-d/2} \rho_{el}(x) dx \right]^2 + k_B T \sum_{i=1}^2 \rho_i g_i \left(-\frac{d+a_i}{2} \right). \quad (38)$$

The osmotic pressure, Π , is defined as

$$\Pi = \Pi^\beta - \Pi^\alpha. \quad (39)$$

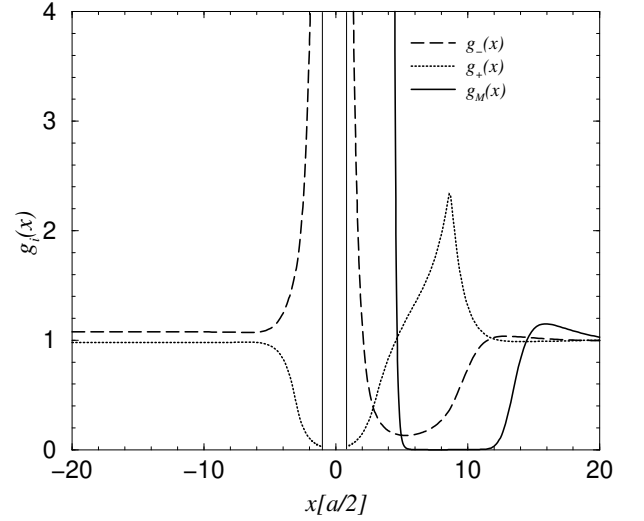


FIG. 2: Reduced concentration profiles (RCPs) for a macroions solution ($\rho_M = 0.01M$, $z_M = -10$) in a monovalent electrolyte ($\rho_+ = 1.1M$ and $\rho_- = 1.0M$), with $a_3 = 3.8a$, $\sigma_1 = \sigma_2 = 0.272$ C/m² and $d = a$. The continuous, dashed and dotted lines represent the RCPs for the macroions, anions and cations, respectively.

From of Eqs. (12), (13), (37) and (38), Eq. (39) becomes,

$$\begin{aligned} \Pi = & \frac{2\pi}{\varepsilon} \{ [\sigma^\beta]^2 - [\sigma^\alpha]^2 \} + k_B T \sum_{i=1}^3 \rho_i g_i \left(\frac{d+a_i}{2} \right) \\ & - k_B T \sum_{i=1}^2 \rho_i g_i \left(-\frac{d+a_i}{2} \right). \end{aligned} \quad (40)$$

Due to the fluid-fluid correlation across a thin membrane, the induced charge densities (σ^α and σ^β) and $g_i \left(\pm \frac{d+a_i}{2} \right)$ depend on the fluid conditions (ρ_i, z_i, a_i , with $i = 1, \dots, 3$) and on the membrane parameters (σ_1, σ_2 and d) [27, 28, 29]. The computed value of Π (using $\sigma^\alpha, \sigma^\beta$ and $g_i \left(\pm \frac{d+a_i}{2} \right)$ from HNC/MS), however, does *not* depend on the membrane parameters. We have numerically corroborated this fact by computing Π for several values of σ_1, σ_2 and d . This is physically appealing since the pressure can only depend on the bulk fluid conditions at both sides of the membrane. However, we had to do very precise calculations of $g_i(x)$, particularly in the neighborhood of $x = \pm \frac{d+a_i}{2}$, to prove the above statement.

Eq. (40) is an *exact* theorem to compute the osmotic pressure, Π , in terms of microscopic quantities. A similar expression for the osmotic pressure was derived by Zhou and Stell [25]. However, the differences between the current derivation and that of those authors are due to the ions-membrane short range interactions. If we use, in the Zhou and Stell theory, the hard wall interaction between the permeable ions and the membrane (provided by Eq. (16)) we recover Eq. (40).

III. RESULTS AND DISCUSSION

Several physical effects determine particles adsorption on the charged membrane. One of the most relevant is the membrane-particle direct interaction energy, which, at the surface is given by

$$U_i = q_i u_i \left(\frac{a_i}{2} \right) = \frac{2\pi q_i \sigma}{\varepsilon} \left(L - \frac{a_i}{2} \right), \quad (41)$$

being L the location of a reference point. The more negative the value of $U_i < 0$, particles adsorption is energetically more favorable. Many body correlations play also an important role in the adsorption phenomena and are responsible for the surface-particle forces of non-electrostatic origin. Although it is not possible to sharply distinguish the origin of correlations, we assume that the particles volume fraction ($\eta_T \equiv \frac{\pi}{6} \sum_i \rho_i a_i^3$) quantifies the contribution of short range correlations. To quantify the effect of the coulombic interaction (long range correlations), we define the parameter $\xi_{ij} = \beta q_i q_j / \varepsilon a_{ij}$ and we simply write $\xi_i \equiv \xi_{ii} = \beta q_i^2 / \varepsilon a_i$, when $i = j$. In the discussion, the effects produced by varying the fluid parameters (a_i , z_i and ρ_i , with $i = 1, \dots, 3$) will be associated with the increment (or decrement) of the contributions arising from short and long range correlations (η_T and ξ_{ij}).

For our discussion it is useful remark the following concepts: When the amount of adsorbed charge exceeds what is required to screen the surface charge, it is said to occur a surface *charge reversal* (CR). In consequence, at certain distance from the surface the electric field is inverted. Next to the CR layer, a second layer of ions (with same charge sign as that of the surface) is formed, producing a *charge inversion* (CI) of the electrical double layer [48, 49]. Such a denomination (charge inversion) is originated from the fact that ions invert their role in the diffuse layer. In the past, we have shown that charge reversal and charge inversion are many body effects and are induced by a compromise between short range correlations (η_T) and electrostatic long range correlations (ξ_{ij}) [37, 50].

The HNC/MS equations for a semipermeable membrane, Eqs. (19), are numerically solved using a finite element technic [51, 52]. From the solution of HNC/MS equations the reduced concentration profiles (RCPs), $g_j(x)$, are obtained. In the discussion, we adopted the following notation: $z_1 = z_+$, $z_2 = z_-$ and $z_3 = z_M$ for the number valence of cations, anions and macroions, respectively; idem for ρ_i and a_i . In all our calculations we have used fixed values of $T = 298\text{K}$, $\varepsilon = 78.5$ and $a = 4.25 \text{ \AA}$. The effects of salt valence, macroions size, and membrane surface charge density on macroions adsorption are analyzed. Thus, we consider macroions ($\rho_M = 0.01\text{M}$ and $z_M = 10$) in a (a) monovalent ($\rho_+ = 1.1\text{M}$ and $\rho_- = 1.0\text{M}$) and (b) divalent ($\rho_+ = 0.55\text{M}$ and $\rho_- = 0.5\text{M}$) electrolyte solutions. For each case, we considered two macroion sizes ($a_M = 3.8a$ and $a_M = 7a$)

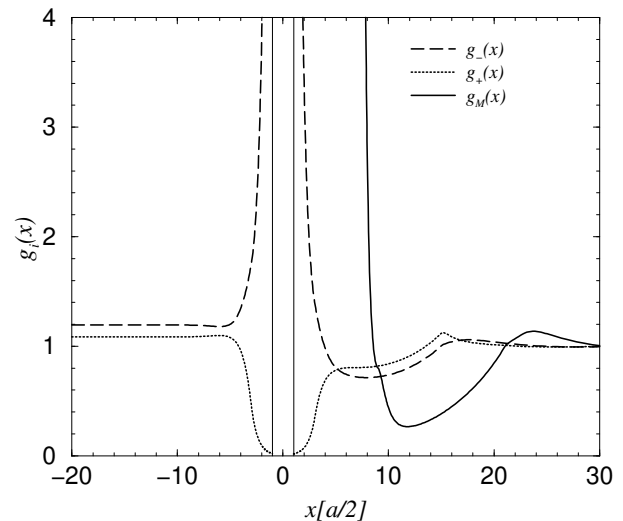


FIG. 3: Same as in Fig. 2 but with $a_3 = 7a$. The lines meaning is the same as in Fig. 2

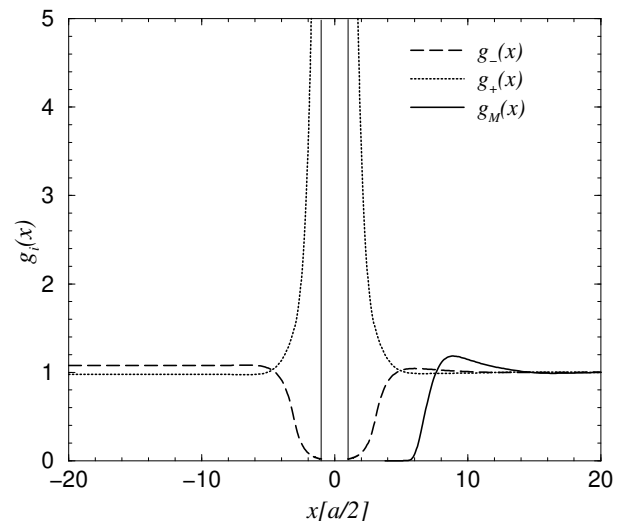


FIG. 4: Reduced concentration profiles (RCPs) for a macroions solution ($\rho_M = 0.01\text{M}$, $z_M = -10$) in a monovalent electrolyte ($\rho_+ = 1.1\text{M}$ and $\rho_- = 1.0\text{M}$), with $a_3 = 3.8a$, $\sigma_1 = \sigma_2 = -0.272 \text{ C/m}^2$ and $d = a$. The lines meaning is the same as in Fig. 2

and three values for the membrane charge densities: i) $\sigma_1 = \sigma_2 = 0.272\text{C/m}^2$, ii) $\sigma_1 = \sigma_2 = -0.272\text{C/m}^2$ and iii) $\sigma_1 = 0.68\text{C/m}^2$, $\sigma_2 = -0.136\text{C/m}^2$. Finally we show calculations for the osmotic pressure (as a function of the macroion concentration) compared with experimental results.

A. Macroions in a monovalent electrolyte ($z = 1$)

In this subsection we discuss the case of macroions ($z_M = -10$) in a monovalent electrolyte solution ($\rho_+ =$

1.1M, $\rho_- = 1.0M$, $z_+ = -z_- = 1$).

1. Positively charged membrane

In Fig. 2 we present the RCPs when the membrane is positive and symmetrically charged ($\sigma_1 = \sigma_2 = 0.272C/m^2$), the membrane thickness is $d = a$ and $a_M = 3.8a$. As a result, we obtained the asymptotic values of the distribution functions in the α -phase, $g_-(-\infty) = 1.0758$ and $g_+(-\infty) = 0.9779$, such that Eq. (10) is satisfied. In both phases we observe that the negative ions are adsorbed and the positive ions expelled, as it is expected. In the β -phase we observe that the adsorption of macroions is more favorable than the adsorption of negative small ions. This is understood in terms of the electrostatic energy of one particle of species i at the membrane surface, U_i : since $|z_M| > |z_-|$, from Eq. (41) it is easy to see that $U_M < U_- < 0$, which favors macroions adsorption. As we pointed out above, many body correlations also influence adsorption. In this case macroion-macroion long range correlations are predominantly more important than the ion-ion correlations since $\xi_M \approx 7\xi_-$. Short range correlations are also important and play an important role in the macroions adsorption: an increment of macroions concentration (keeping constant a_M and z_M) implies an increment of η_T and produces an increment of the macroions adsorption. However an increment of η_T not always is followed by an increase of the adsorption as it will be noticed in the discussion of Fig. 3. In the macroions RCP we find a first macroions layer next to the membrane surface, after this layer there is a region where the macroions are completely expelled and then a small second peak. The negative small ions are also adsorbed to the membrane's surface but their concentration is smaller than for the macroions. The RCP for positive ions show that these are completely expelled from the membrane right surface. However, a peak in the RCP is found at $x \approx 4.3a$ which is the ion-surface distance when there is a macroion in between. This peak implies an effective surface-cation attraction due to a *field inversion* caused by the surface CR.

Fig. 3 shows the results obtained for the same system as in Fig. 2 except that the macroions are larger, $a_M = 7a$. At the α -phase the distribution function have the same qualitative behavior as in Fig. 2, however, in this case $g_-(-\infty) = 1.1938$ and $g_+(-\infty) = 1.0853$, i. e., the amount of salt in the α -phase increases by increasing the macroions size. Respect to Fig. 2, a decrement of macroions adsorption is observed in Fig. 3. The increment of the macroions diameter implies a decrement of the macroions-macroions long range correlations (in this case $\xi_M \approx 2\xi_-$) and an increment of η_T , and hence, an increment of the contributions arising from correlations of short range nature. Such an increment, however, does *not* increase (but decrease) the macroions adsorption. This is understood in terms of Eq. (41)

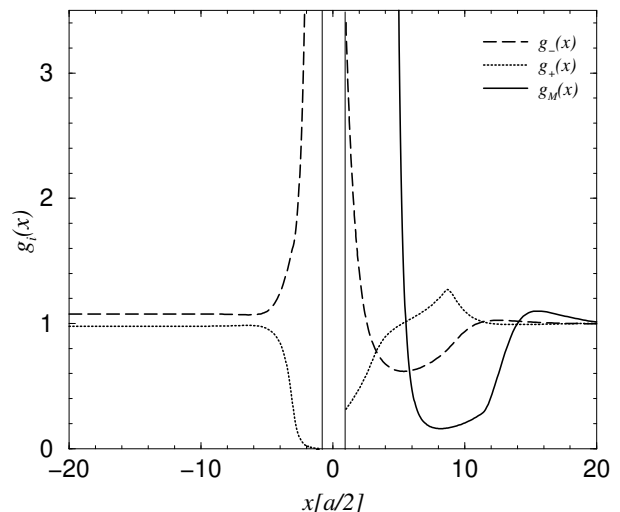


FIG. 5: Reduced concentration profiles (RCPs) for a macroions solution ($\rho_M = 0.01M$, $z_M = -10$) in a monovalent electrolyte ($\rho_+ = 1.1M$ and $\rho_- = 1.0M$), with $a_3 = 3.8a$, $\sigma_1 = 0.68 C/m^2$, $\sigma_2 = -0.136 C/m^2$ and $d = a$. The lines meaning is the same as in Fig. 2.

[$U_M(a_M = 3.8a) < U_M(a_M = 7a)$] which implies that the adsorption is energetically less favorable for $a_M = 7$ than for smaller macroions with the same charge.

2. Negatively charged membrane

Fig. 4 shows the RCPs when the membrane is negative and symmetrically charged ($\sigma_1 = \sigma_2 = -0.272C/m^2$) for $a_M = 3.8a$. The membrane thickness is $d = a$. The asymptotic value of the distributions function does not depend on the membrane's charge and thickness, hence, the $g_i(-\infty)$ have the same value as in Fig. 2. The RCP for small ions behave in a normal way in the sense that positive ions are attracted to the to the membrane surface, whereas the negative ions are expelled from it. In the β -phase, it is observed that macroions are expelled from the membrane surface for $x < 6(a/2)$. After this zero concentration region, a small peak in the macroions RCP is observed at $x \approx 9(a/2)$ indicating an effective macroion-membrane *attractive* force and a slight surface CR produced by the small cations. At these electrolyte conditions (1 : 1 and $\rho_+ = 1M$ with no macroions), cations display a monotonically decaying distribution profile [12], hence, the oscillatory behavior of the RCPs for the small ions (in the β -phase) is a consequence of the presence of macroions. By considering the macroions size $a_M = 7.0$ (not shown), the qualitative behavior of the RCPs is similar to that of Fig. 4 with the following differences: (i) the RCPs oscillations of the small ions at the β -phase are of longer range and (ii) the macroions RCP maximum is higher. This fact points out the relevance of the effect of the particles size and concentration (particles volume fraction) in the effec-

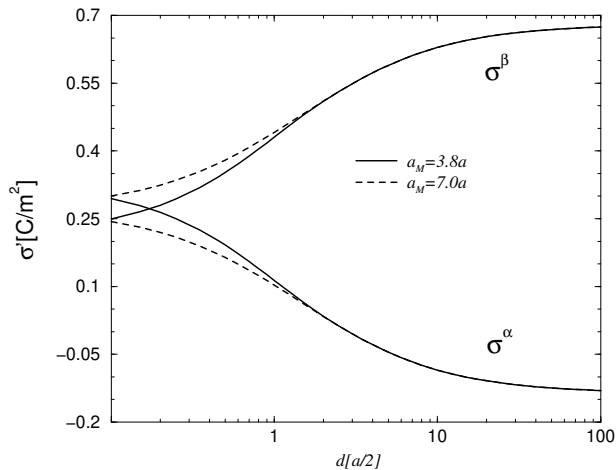


FIG. 6: Induced charge densities as a function of the membrane thickness for a macroions solution ($\rho_M = 0.01\text{M}$, $z_M = -10$) in a monovalent electrolyte ($\rho_+ = 1.1\text{M}$ and $\rho_- = 1.0\text{M}$) with $\sigma_1 = 0.68\text{ C/m}^2$ and $\sigma_2 = -0.136\text{ C/m}^2$. The continuous line represents calculations for $a_M = 3.8a$, whereas the dashed line for $a_M = 7.0a$

tive attraction between like charged particles in solution [30, 31, 32, 33, 34].

From the analysis presented from Fig. 2 to 4 we see that macroions adsorption increases by increasing η_T , ξ_M and $-U_M$. However, we point out the following findings: when macroions and the surface are oppositely charged, long range electrostatic correlations dominate over short range correlations. Hence, adsorption is enhanced by increasing ξ_M and/or $-U_M$. On the other hand, when macroions and the surface are like charged the mechanism for macroions adsorption (mediated by the small ions) is mainly driven by short range correlations, thus, adsorption increases by increasing η_T even though ξ_M decreases.

3. Unsymmetrically charged membrane

In Fig. 5 it is shown the RCPs at the two membrane sides for a macroions diameter $a_3 = 3.8a$ and $d = a$. The membrane is *unsymmetrically* charged with $\sigma_1 = 0.68\text{ C/m}^2$ and $\sigma_2 = -0.136\text{ C/m}^2$. At the right hand side surface macroions and small anions (negatively charged) are adsorbed on the membrane, in spite of $\sigma_2 < 0$. The adsorption of negatively charged particles on a negatively charged surface is due to the correlation between the two fluids. This is understood by considering the following two facts: (i) the membrane has a positive *net* charge ($\sigma_T > 0$) and (ii) the charge on the left hand side surface (σ_1) is not completely screened by the excess of charge in its corresponding fluid phase (σ^α), therefore, the electric field produced by $\sigma_1 + \sigma^\alpha$ overcomes the field produced by σ_2 , inducing macroions and anions adsorption. From here, we observed that σ^α and σ^β depend on d as it is

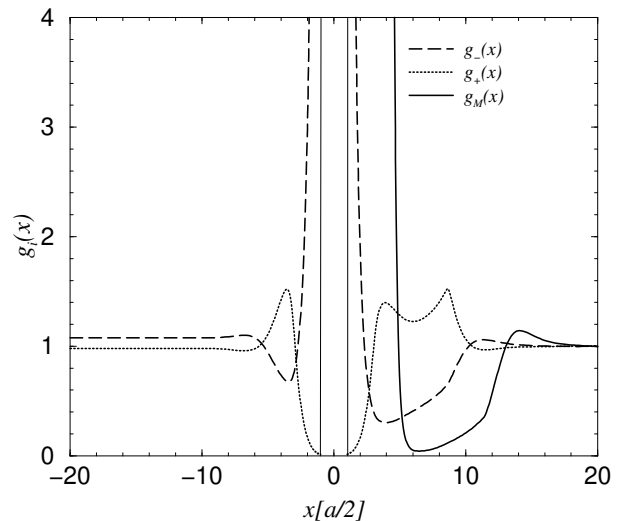


FIG. 7: Reduced concentration profiles (RCPs) for a macroions solution ($\rho_M = 0.01\text{M}$, $z_M = -10$) in a divalent electrolyte ($\rho_+ = 0.55\text{M}$ and $\rho_- = 0.5\text{M}$), with $a_3 = 3.8a$, $\sigma_1 = \sigma_2 = 0.272\text{ C/m}^2$ and $d = a$. The continuous, dashed and dotted lines represent the RCPs for the macroions, anions and cations, respectively.

discussed below.

In Fig. 6 it is shown the excess of charge densities σ_α and σ_β , as a function of the membrane's thickness d . The dependence on the wall thickness of the induced charge densities σ_α and σ_β , is a manifestation of the correlation between the fluids. The correlation between the two fluids is due to the electrostatic interaction among the particles at both phases but, more importantly, to the fact that they are at constant chemical potential. For a sufficiently large membrane's thickness the induced charge density in each fluid phase screens its corresponding membrane surface, i. e., $\sigma^\alpha \rightarrow -\sigma_1$ and $\sigma^\beta \rightarrow -\sigma_2$ as $d \rightarrow \infty$. At $d = 100a$ each fluid has screened its respective surface charge density. Here we show a comparison between the results obtained for $a_M = 3.8a$ and $a_M = 7a$. In both cases the results are qualitatively similar.

B. Macroions in a divalent electrolyte ($z = 2$)

We now discuss the case of macroions ($z_M = -10$) in a divalent electrolyte solution ($\rho_+ = 0.55\text{M}$, $\rho_- = 0.5\text{M}$, $z_+ = -z = 2$).

1. Positively charged membrane

In Fig. 7 we show the RCPs for $\sigma_1 = \sigma_2 = 0.272\text{C/m}^2$, $d = a$ and $a_M = 3.8a$. At the α -phase we observe oscillations of the RCPs, which is a typical behavior of a divalent electrolyte. Although we observe a strong adsorption of macroions in the β -phase, the amount of ad-

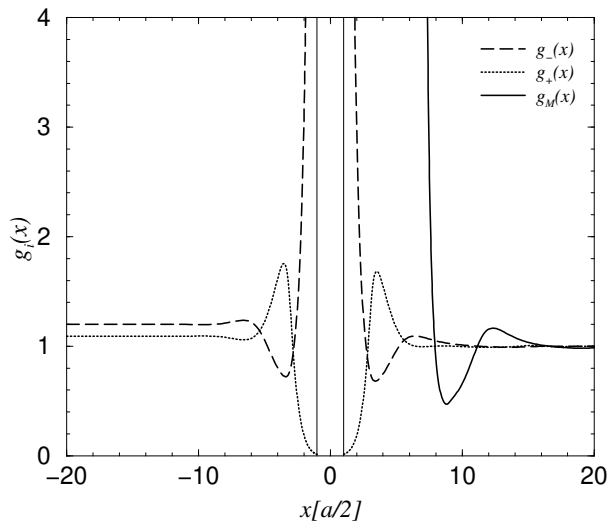


FIG. 8: Same as in Fig. 7 but with $a_3 = 7a$. The lines meaning is the same as in Fig. 7.

sorbed small negative ions is even larger (the concentrations of macroions and small negative ions at the interface are $\rho_M \left(\frac{d+a_M}{2}\right) \approx 7.2\text{M}$ and $\rho_- \left(\frac{d+a}{2}\right) \approx 16\text{M}$, respectively). Energetically, macroions adsorption should be more favorable, however, macroions adsorption is inhibited because divalent positive ions more efficiently screen macroion-membrane and macroion-macroion interactions. We infer this from the RCP for cations, which displays two small peaks at $x \approx 2a$ and $x \approx 4.3a$. The first peak corresponds to a positive ions layer contiguous to the negative ions adsorbed on the wall. The position of the second peak corresponds to a positive ions layer next to the macroions layer. This structure indicates that positive ions surround macroions due to their strong electrostatic interaction, in this case $\xi_{M+} \approx -8.3 \frac{e^2}{\epsilon k_B T a} \approx -14$, whereas for macroions in a monovalent electrolyte $\xi_{M+} \approx -7$. By comparison of Figs. 2 and 7 we see that macroions (next to an oppositely charged surface) are better adsorbed when they are in a monovalent solution rather than in a multivalent solution: for this particular case of macroions ($\rho_M = 0.01\text{M}$, $z_M = -10$ and $a_M = 3.8a$), $\rho_M \left(\frac{d+a_M}{2}\right) = 20\text{M}$ when macroions are in a monovalent electrolyte, whereas $\rho_M \left(\frac{d+a_M}{2}\right) \approx 7.2\text{M}$ when macroions are in a divalent electrolyte.

In Fig. 8 we show the RCPs for the same conditions as in Fig. 7 but $a_M = 7a$. Although macroions adsorb in the β -phase, they do not influence significantly on the local concentration of small ions. Hence, we see that the RCPs for small ions are quantitatively similar in both phases: the concentrations of counterions at the membrane surfaces are $\rho \left(\pm \frac{d+a}{2}\right) \approx 22.5\text{M}$, in addition, the RCPs maxima are located symmetrically around $x \approx \pm 1.7a$. The adsorption of macroions decrease (respect to Fig. 7) due to the efficient screening of the membrane charge by the small negative ions and because the adsorption of larger ions (keeping z_M constant) is energetically less favorable,

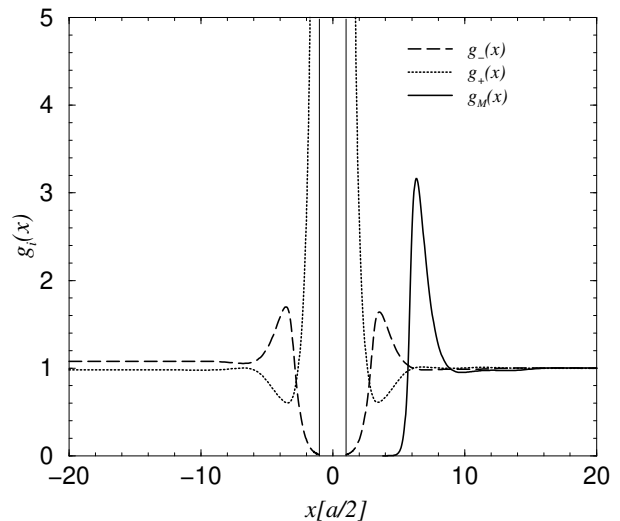


FIG. 9: Reduced concentration profiles (RCPs) for a macroions solution ($\rho_M = 0.01\text{M}$, $z_M = -10$) in a divalent electrolyte ($\rho_+ = 0.55\text{M}$ and $\rho_- = 0.5\text{M}$), with $a_3 = 3.8a$, $\sigma_1 = \sigma_2 = -0.272 \text{ C/m}^2$ and $d = a$. The lines meaning is the same as in Fig. 7.

as it was pointed out in the discussion of Fig. 3. We see that the layer of cations around macroions (seen in Fig. 7) disappears due to the decrement of their coulombic interaction, in this case $\xi_{M+} \approx -7.6$.

2. Negatively charged membrane

In Fig. 9 we show the RCPs for a negatively charged membrane ($\sigma_1 = \sigma_2 = -0.272\text{C/m}^2$) with $d = a$ and $a_M = 3.8a$. The quantitative behavior of the small ions RCPs is similar at both phases, as much as the location of the maxima located symmetrically at $x \approx \pm 1.8a$. At the β -phase, the macroions RCP displays a peak at $x = 3.2a$ indicating the formation of a macroions layer. The *adsorption* of macroions at this layer is enhanced (respect to Fig. 4) because of the surface *charge reversal* produced by the divalent cations, i. e., macroions see the membrane surface with an effective positive charge. By increasing macroions size (keeping z_M constant), macroions attraction to an oppositely charged surface is energetically less favorable, thus, we observe that macroions adsorption decreases by increasing macroions size, in opposition to the behavior of macroions in a monovalent electrolyte.

It seems to be a general feature that macroions next to an oppositely charged surface are better adsorbed when they are in a monovalent solution than in a multivalent solution. It is important to point out the formation of a cations layer around the macroions when $|\xi_{M+}|$ is high (seen for divalent electrolyte in Fig. 7). On the other hand, when macroions and the surface are like charged, a *divalent* electrolyte solution mediates an effective membrane-macroions attraction, this attraction

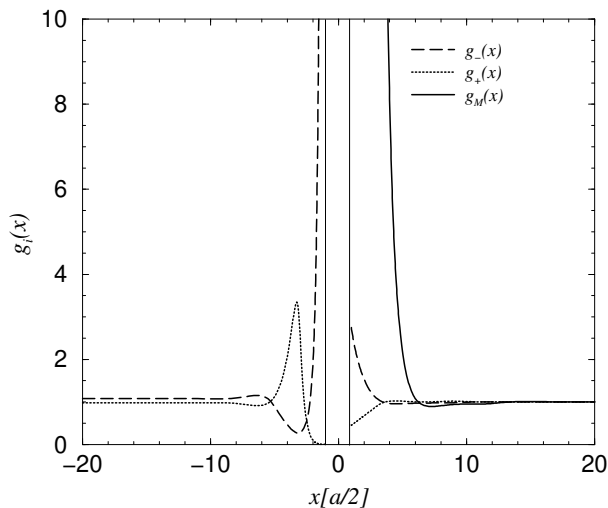


FIG. 10: Reduced concentration profiles (RCPs) for a macroions solution ($\rho_M = 0.01\text{M}$, $z_M = -10$) in a divalent electrolyte ($\rho_+ = 0.55\text{M}$ and $\rho_- = 0.5\text{M}$), with $a_3 = 3.8a$, $\sigma_1 = 0.68 \text{ C/m}^2$, $\sigma_2 = -0.136 \text{ C/m}^2$ and $d = a$. The lines meaning is the same as in Fig. 7.

is favored by a higher value of ξ_M rather than for a high value of η_M , as in the monovalent case.

3. Unsymmetrically charged membrane

In Fig. 10 we show the RCPs at the two phase for $\sigma_1 = 0.68\text{C/m}^2$, $\sigma_2 = -0.136\text{C/m}^2$, $a_3 = 3.8a$ and $d = a$. The correlation between the two fluids is manifested by the attraction of negatively charged particles towards the negatively charged surface at the α -phase. However, the adsorption of macroions is quite less efficient than in the monovalent electrolyte case of Fig. 5: In the monovalent case the contact value of the local concentration is $\rho_M(\frac{d+a_M}{2}) \approx 2.7\text{M}$ whereas in this case it is $\rho_M(\frac{d+a_M}{2}) \approx 0.12\text{M}$. This is due mainly to the more efficient field screening by the divalent electrolyte at the left hand side surface. In the monovalent electrolyte case the induced charge density at the α -phase is $\sigma_\alpha = -0.43\text{C/m}^2$ when $d = a$ whereas in the divalent electrolyte case $\sigma_\alpha = -0.50\text{C/m}^2$.

C. The osmotic pressure

Although the adsorption of macroions is strongly influenced by the membrane surface charge and thickness, we observe however, that the osmotic pressure does not depend on these membrane properties as it has been pointed out in subsection II C. In Fig. 11 we show the osmotic pressure (obtained from HNC/MS theory) as a function of the macroions concentration ρ_M , for two macroion sizes. This plot shows the osmotic pressure for

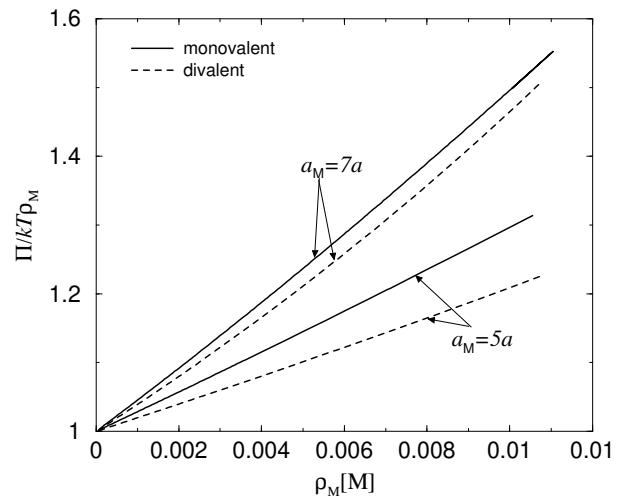


FIG. 11: Reduced osmotic pressure as a function of the macroions concentration, ρ_M , for $z_M = -10$ and two macroion sizes, $a_M = 5a$ and $a_M = 7a$. The solid line represents the osmotic pressure for macroions in a monovalent electrolyte ($\rho_- = 1.0\text{M}$) whereas the dashed line for macroions in a divalent electrolyte ($\rho_- = 0.5\text{M}$).

macroions in a monovalent electrolyte and in a divalent electrolyte. The osmotic pressure increases by increasing the particles excluded volume (either ρ_M or a_M), on the other hand, it is not observed a qualitative difference between the curves for the osmotic pressure of macroions in a monovalent and divalent electrolytes.

Computation of the osmotic pressure of proteins solutions is an issue addressed by some authors [7, 53]. Results of particular interest are those for albumin solutions, for which theoretical calculations and measurements of the osmotic pressure have been reported. In Fig. 12 we show the osmotic pressure predictions of HNC/MS theory (as a function of the protein concentration) and experimental results. The experimental data correspond to a solution of albumin in a 0.15M NaCl aqueous solution. In accordance with titration measurements, the albumin has a net charge of $Q = -9e$ and $Q = -20e$ for $\text{pH} \approx 5.4$ and $\text{pH} \approx 7.4$, respectively, in our calculations we have used $a_M = 62\text{\AA}$ which corresponds to the experimental protein diameter. It is remarkable the excellent agreement between theory and experiment as well as the fact that no adjustable parameters have been used. The prediction of HNC/MS fits well the experimental data even for protein concentration as high as 30% the protein volume in solution (which is estimated assuming the albumin molecular weight $w_{al} = 69\text{Kg/mol}$). For higher protein concentration, HNC/MS shows discrepancies with experimental measurements which may be associated with the following facts: (i) the albumin molecule is not *spherically* symmetric as in the model, therefore, the protein geometry becomes relevant when the protein volume fraction is high, (ii) integral equations are approximated theories,

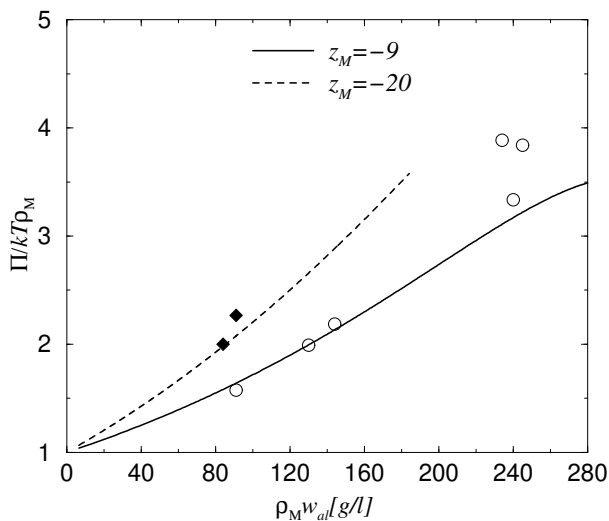


FIG. 12: Bovine serum albumin reduced osmotic pressure as a function of albumin weight concentration, $\rho_M w_{al}$, at 25°C and in 0.15M NaCl at $\text{pH}=7.4$ ($Q = -20e$) and $\text{pH}=5.4$ ($-9e$) from ref. [6]. The curves are obtained from Eq. (12) using $a_M = 62\text{\AA}$, $a = 4.25\text{\AA}$ and $z = 1$.

meaning that they do not take into account all the particle correlations.

IV. CONCLUSIONS

We studied a model charged membrane separating two fluid phases (α and β). The β -phase contains macroions in an electrolyte solution and the α -phase is a simple electrolyte solution. The system is modeled in such a way that the small ions at both phases are at the same chemical potential, thus, the membrane is considered to be semipermeable. It is important to point out that we considered explicitly the effect of particles size (short range correlations) and electrostatic long range correlations. Here we have applied the hypernetted chain/mean spherical integral equations to the semipermeable membrane model. Also we have derived the equation for the osmotic pressure through a simple forces balance.

By solving the HNC/MS integral equations we obtained the particles concentration profiles which allowed us to study the adsorption of macroions on the membrane. We analyzed the influence of several factors in the macroions adsorption: membrane surface charge, membrane thickness, the effect of salt and macroions size. From this study we emphasize the following results: 1) When the membrane and macroions are oppositely charged the adsorption is energetically favorable, however, if multivalent ions are present the membrane-macroions interaction is screened which is unfavorable for macroions adsorption. On the other hand, the larger the macroions (keeping the same charge and concentra-

tion) the adsorption is energetically less favorable. 2) The attraction of macroions towards a like-charged surface seems to be energetically unfavorable. Nevertheless, in our model, we find that such an attraction is feasible and it is due to short range correlations, which are properly considered in our theory. These previous results are not a consequence of the permeability condition but are general. 3) As a consequence of the permeability condition and constant chemical potential, we have that for an unsymmetrically charged membrane the fluids *correlation* may produce adsorption of charged macroions on a like charged surface. In addition, the permeability condition implies a non trivial relation between the induced charge densities (σ^α and σ^β) and the membrane thickness. The theory predictions are robust as it is shown by the excellent agreement between theory and experiment where we have not used adjustable parameters. The results of this work could be technologically relevant for the design of selective membranes [54].

V. ACKNOWLEDGMENTS

We gratefully acknowledge the financial support of INDUSTRIAS NEGROMEX.

APPENDIX A: APPENDIX

1. The Mean Spherical Closure

The primitive model is the simplest model for an electrolyte that includes many relevant aspects of real solutions. In the general case the primitive model is constituted by n -species of particles, with the mixture is embedded in a uniform medium of dielectric constant ϵ at temperature T . Each species is defined by the particles point charge at the center, $q_i = z_i e$ (where e stands for the proton's charge and z_i for the ionic valence), the ionic diameter, a_i , and number concentration, ρ_i . The fluid is constrained to the following condition

$$\sum_{i=1}^n z_i \rho_i = 0. \quad (\text{A1})$$

The expressions for the direct correlation functions, $c_{ij}(r_{13})$, for a *bulk* electrolyte (required in n Eq. (7)) were obtained by Blum [55] and Hiroike [56], through the MS closure, and are written as

$$c_{ij}(r_{13}) = \frac{e^2 \beta}{\epsilon} d_{ij}(r_{13}) + c_{ij}^{hs}(r_{13}) - \beta \frac{z_i z_j e^2}{\epsilon r_{13}}, \quad (\text{A2})$$

with $c_{ij}^{sr}(r_{13}) = \frac{e^2\beta}{\varepsilon}d_{ij}(r_{13})$, $\beta = 1/k_B T$ and

$$d_{ij}(r_{13}) = \begin{cases} b_{ij}^{(1)} + \frac{z_i z_j}{r_{13}}, & \text{for } 0 \leq r_{13} \leq \lambda_{ij}, \\ \frac{b_{ij}^{(2)} + z_i z_j}{r_{13}} - b_{ij}^{(3)} + b_{ij}^{(4)} r_{13} + b_{ij}^{(5)} r_{13}^3, & \text{for } \lambda_{ij} < r_{13} \leq a_{ij}, \\ 0, & \text{for } r_{13} > a_{ij}; \end{cases} \quad (\text{A3})$$

with $\lambda_{ij} \equiv \frac{|a_i - a_j|}{2}$ and $a_{ij} \equiv \frac{a_i + a_j}{2}$. The constants in Eq. (A3) are given by

$$\begin{aligned} s_i &= (n_i + \Gamma x_i), \\ b_{ij}^{(1)} &= 2[z_i n_j - x_i s_i + \frac{a_i}{3} s_i^2], \\ b_{ij}^{(2)} &= (a_i - a_j) \left\{ \frac{(x_i + x_j)}{4} [s_i - s_j] \right. \\ &\quad \left. - \frac{(a_i - a_j)}{16} [(n_i + \Gamma x_i + n_j + \Gamma x_j)^2 - 4n_i n_j] \right\}, \\ b_{ij}^{(3)} &= (x_i - x_j)(n_i - n_j) \\ &\quad + (x_i^2 + x_j^2) \Gamma + (a_i + a_j) n_i n_j - \frac{1}{3} [a_i s_i^2 + a_j s_j^2], \\ b_{ij}^{(4)} &= \frac{x_i}{a_i} s_i + \frac{x_j}{a_j} s_j + n_i n_j - \frac{1}{2} [s_i^2 + s_j^2], \\ b_{ij}^{(5)} &= \frac{s_j}{6a_j^2} + \frac{s_i}{6a_i^2}, \end{aligned}$$

where x_i are defined as $x_i \equiv z_i + n_i a_i$ and Γ is obtained from the solution of the following algebraic equation

$$\Gamma^2 = \frac{\pi e^2 \beta}{\varepsilon} \sum_{i=1}^n \rho_i (z_i + n_i a_i)^2. \quad (\text{A4})$$

The n_i are obtained from the solution of the following set of algebraic equations

$$-(z_i + n_i a_i) \Gamma = n_i + c a_i \sum_{j=1}^n (z_j + n_j a_j), \quad (\text{A5})$$

where $c = \frac{\pi}{2} [1 - \frac{\pi}{6} \sum_{j=1}^n \rho_j a_j^3]^{-1}$.

Considering that $a = a_1 = a_2$, $c_{ij}^{hs}(r_{13})$ is just the direct correlation function for a hard spheres *binary* mixture in the PY approximation. For particles of the same size it is given by [57]

$$c_{ii}^{hs}(r_{13}) = \begin{cases} -A_i - B_i r_{13} - \delta r_{13}^3 & \text{for } r_{13} < a_i, \\ 0, & \text{for } r_{13} > a_i. \end{cases} \quad (\text{A6})$$

For particles of different size we have

$$c_{13}^{hs}(r_{13}) = \begin{cases} -A_1 & \text{for } s \leq \lambda_{13}, \\ -A_1 - \frac{[\alpha x^2 + 4\lambda_{13} \delta x^3 + \delta x^4]}{r_{13}} & \text{for } \lambda_{13} < r_{13} \leq a_{13}, \\ 0 & \text{for } r_{13} > a_{13}. \end{cases} \quad (\text{A7})$$

with $x \equiv r_{13} - \lambda_{13}$. The constants used in Eqs. (A6) and (A7) are given by

$$\begin{aligned} A_1 &= (1 - \eta_T)^{-3} \left\{ 1 + \eta_T + \eta_T^2 + \frac{\pi}{6} a^3 \rho_T [1 + 2\eta_T] \right. \\ &\quad \left. - \frac{\pi}{2} \rho_3 (a_3 - a)^2 \{ a(1 + \eta_3) + a_3 [1 + 2(\eta_1 + \eta_2)] \} \right\} \\ &\quad + \frac{\pi a^3}{2} (1 - \eta_T)^{-4} \{ \rho_T (1 + \eta_T + \eta_T^2) \\ &\quad - \frac{\pi}{2} \rho_3 (\rho_1 + \rho_2) (a_3 - a)^2 [(a + a_3) + a a_3 \frac{\pi}{6} \sum_{i=1}^3 \rho_i a_i^2] \}, \end{aligned} \quad (\text{A8})$$

$$\alpha = -\pi a_{13} g_{13}(a_{13}) \sum_{i=1}^3 \rho_i a_i g_{ii}(a_i), \quad (\text{A9})$$

$$\delta = \frac{\pi}{12} \sum_{i=1}^3 \rho_i A_i, \quad (\text{A10})$$

$$B_1 = B_2 = -\pi [(\rho_1 + \rho_2) a^2 g_{11}^2(a) + \rho_3 a_3 g_{13}^2(a_{13})], \quad (\text{A11})$$

with

$$\begin{aligned} g_{11}(a) = g_{22}(a) &= \left\{ \left[1 + \frac{1}{2} \eta_T \right] + \frac{3}{2} \eta_3 a_3^3 (a - a_3) \right\} (1 - \eta_T)^{-2}, \\ g_{13}(a_{13}) &= \frac{[a_3 g_{11}(a) + a g_{33}(a_3)]}{2a_{13}}. \end{aligned} \quad (\text{A12})$$

The expressions for A_3 , B_3 and $g_{33}(a_3)$ are obtained by interchanging $\eta_1 + \eta_2$, $\rho_1 + \rho_2$ and a_1 with η_3 , ρ_3 and a_3 , respectively, in the expressions for A_1 , B_1 , $g_{11}(a)$.

2. The kernels expressions

Carrying out the integrations indicated in Eqs. (21) and (22), using Eqs. (A3), (A6) and (A7), the expressions for $K_{ij}(x, y)$ and $D_{ij}(x, y)$ are

$$D_{ij}(x, y) = \begin{cases} b_{ij}^{(1)} k_0 + z_i z_j J_1 + b_{ij}^{(2)} M_1 - b_{ij}^{(3)} M_2 + b_{ij}^{(4)} M_3 + b_{ij}^{(5)} M_5, & \text{for } 0 \leq |x - y| \leq \lambda_{ij}, \\ (b_{ij}^{(2)} + z_i z_j) J_1 - b_{ij}^{(3)} J_2 + b_{ij}^{(4)} J_3 + b_{ij}^{(5)} J_5, & \text{for } \lambda_{ij} < |x - y| \leq a_{ij}, \\ 0, & \text{for } a_{ij} < |x - y| \end{cases} \quad (\text{A13})$$

$$-K_{ii}(x, y) = \begin{cases} A_i J_2 + B_i J_3 + \delta J_5, & \text{for } a_{ii} \geq |x - y|, \\ 0, & \text{for } a_{ii} < |x - y|, \end{cases} \quad (\text{A14})$$

$$-K_{13}(x, y) = \begin{cases} A_1 J_2 + \alpha a^3 / 3 + \delta \lambda_{13} a^4 + \delta a^5 / 5, & \text{for } |x - y| < \lambda_{13}, \\ A_1 J_2 + \nu P_3 + 4\delta \lambda_{13} P_4 + \delta P_5, & \text{for } \lambda_{13} < |x - y| \leq a_{13}, \\ 0, & \text{for } a_{13} < |x - y|, \end{cases} \quad (\text{A15})$$

where we use the following definitions:

$$J_n = (a_{ij}^n - |x - y|^n) / n, \quad (\text{A16})$$

$$P_n = (a^n - (|x - y| - \lambda_{ij})^n) / n, \quad (\text{A17})$$

$$M_n = (a_{ij}^n - \lambda_{ij}^n) / n, \quad (\text{A18})$$

and

$$k_0 = (\lambda_{ij}^2 - (x - y)^2) / 2. \quad (\text{A19})$$

-
- [1] Hoppe, W. *Biophysics*; Springer Verlag, Berlin, 1983.
- [2] Hiemenz, P. C. *Principles of Colloids and Surface Chemistry*; Marcel Dekker, Inc., New York, 1977.
- [3] Tanford, C. *Physical Chemistry of Macromolecules*; Jhon Wiley and Sons, Inc., New York, 1961.
- [4] Donnan, F. G. Z. *Elektrochem.* **1911**, *17*, 572.
- [5] Guggenheim, E. A. *Thermodynamics: An Advanced Treatment for Chemists and Physicists*; North Holland Physics Publishing, Amsterdam, 1967.
- [6] Vilker, V. L.; Colton, C. K.; Smith, K. A. *J. of Coll. Int. Sci.* **1980**, *79*, 548.
- [7] Yousef, M. A.; Datta, R.; Rodgers, V. G. J.; *J. of Coll. Int. Sci.* **1998**, *207*, 273.
- [8] Gouy, G. *J. Phys.* **1910**, *9*, 457.
- [9] Chapman, D. L. *Philos. Mag.* **1913**, *25*, 475.
- [10] Cuvillier, N.; Rondelez, F.; *Thin Solid Films* **1998**, *327-329*, 19.
- [11] Torrie, G. M.; Valleau, J. P. *J. Chem. Phys.* **1980**, *73*, 5807.
- [12] Lozada-Cassou, M.; Saavedra-Barrera, R.; Henderson, D. *J. Chem. Phys.* **1982**, *77*, 5150.
- [13] Svensson, B.; Woodward, B. J. C. E. *J. Phys. Chem.* **1990**, *94*, 2105.
- [14] Percus, J. K. in *The Equilibrium Theory of Classical Fluids*, edited by H. L. Frisch and J. L. Lebowitz; W. A. Benjamin, New York, 1964, Chap. II, p. 33.
- [15] Evans, R. in *Fundamentals of Inhomogeneous Fluids*, edited by D. Henderson; Marcel Dekker Inc., New York, 1992, Chap. 3.
- [16] Zhang, M. Q.; Percus, J. K. *J. Chem. Phys.* **1990**, *92*, 6799.
- [17] Henderson, D.; Abraham, F. F.; Barker, J. A. *Mol. Phys.* **1976**, *31*, 1291.
- [18] Lozada-Cassou, M. *J. Chem. Phys.* **1981**, *75*, 1412.
- [19] Plischke, M.; Henderson, D. *Electrochim. Acta* **1981**, *34*, 1863.
- [20] Greberg, H.; Kjellander, R. *Mol. Phys.* **1994**, *83*, 789.
- [21] Attard, P. *Adv. Chem. Phys.* **1996**, *92*, 1.
- [22] Decher, G. *Science* **1997**, *277*, 1232.
- [23] Tohver, V.; Smay, J. E.; Braun, P. V.; Lewis, J. A. *PNAS* **2001**, *98*, 8950.
- [24] Zhou Y.; Stell, G. *J. Chem. Phys.* **1988**, *89*, 7010.
- [25] Zhou Y.; Stell, G. *J. Chem. Phys.* **1988**, *89*, 7020.
- [26] The cavity is immersed in a two component electrolyte plus one macroion species, where the macroions are restricted to be outside the cavity whereas the electrolyte can permeate it.
- [27] Lozada-Cassou M.; Yu, J.; *Phys. Rev. Lett.* **1996**, *77*, 4019.
- [28] Lozada-Cassou M.; Yu, J.; *Phys. Rev. E* **1997**, *56*, 2958.
- [29] Aguiular, G. E.; Lozada-Cassou, M.; Yu, J. *J. Coll. Int. Sci.* **2002**, *254*, 141.
- [30] Muthukumar, M. *J. Chem. Phys.* **1996**, *105*, 5183.
- [31] Crocker, J. C.; Matteo, J. A.; Dinsmore, A. D.; Yodh, A. G. *Phys. Rev. Lett.* **1999**, *82*, 4352.
- [32] Kepler, G. M.; Fraden, S. *Phys. Rev. Lett.* **1994**, *73*, 356.
- [33] Crocker, J. C.; Grier, D. G. *Phys. Rev. Lett.* **1996**, *77*, 1897.
- [34] Han Y.; Grier, D. G. *Phys. Rev. Lett.* **2003**, *91*, 038302.
- [35] Bolhuis, P. G.; Louis, A. A.; Hansen, J. P. *Phys. Rev. Lett.* **2002**, *89*, 128302.
- [36] Trokhymchuk, A.; Henderson, D.; Nikolov, A.; Wasan, D. T.; *Phys. Rev. E* **2001**, *64*, 012401.
- [37] Jiménez-Ángeles F.; Lozada-Cassou, M. paper in preparation (see cond-mat/0309446 at <http://www.arxiv.org>).
- [38] Lozada-Cassou, M. in *Fundamentals of Inhomogeneous Fluids*, edited by D. Henderson; Marcel Dekker, New York, 1993, Chap. 8.
- [39] Hansen J. P.; McDonald, I. R. *Theory of Simple Liquids*; Academic Press, London, 2nd ed., 1986.
- [40] Degrève, L.; Lozada-Cassou, M.; Sánchez, E.; González-Tovar, E. *J. Chem. Phys.* **1993**, *98*, 8905.
- [41] Lozada-Cassou, M.; Olivares, W.; Sulbarán, B.; *Phys. Rev. E* **1996**, *53*, 522.
- [42] Degrève L.; Lozada-Cassou, M.; *Phys. Rev. E* **1998**, *57*, 2978.
- [43] Deserno, M. ; Jiménez-Ángeles, F.; Holm, C.; Lozada-Cassou, M. *J. Chem. Phys.* **2001**, *105*, 10983.
- [44] Lozada-Cassou, M. *J. Chem. Phys.* **1984**, *80*, 3344.
- [45] Lozada-Cassou M.; Díaz-Herrera, E. *J. Chem. Phys.* **1990**, *92*, 1194.
- [46] Olivares W.; McQuarrie, D. A. *J. Phys. Chem.* **1980**, *84*, 863.
- [47] Carnie S. L.; Chan, D. Y. C. *J. Chem. Phys.* **1981**, *74*, 1293.
- [48] Attard, P. *J. Phys. Chem.* **1995**, *99*, 14174.
- [49] Greberg H.; Kjellander, R. *J. Chem. Phys.* **1998**, *108*, 2940.
- [50] Jiménez-Ángeles F.; Lozada-Cassou, M. paper in preparation (see cond-mat/0303519 at <http://www.arxiv.org>).
- [51] Lozada-Cassou M.; Díaz-Herrera, E. *J. Chem. Phys.* **1990**, *93*, 1386.
- [52] Mier-y-Teeran, L.; Díaz-Herrera, E.; Lozada-Cassou, M.; Saavedra-Barrera, R. *J. Comp. Phys.* **1989**, *84*, 326.
- [53] Deserno M.; von Grünberg, H.-H. *Phys. Rev. E* **2002**, *66*, 011401.
- [54] *Membranes Technology*, edited by S. P. Nunes and K.-V. Peinemann; Wiley-VCH, Weinheim, F. R. G., 2001.
- [55] Blum, L. *Mol. Phys.* **1975**, *30*, 1529.
- [56] Kazuo, H. *Mol. Phys.* **1977**, *33*, 1195.
- [57] Lebowitz, J. L. *Phys. Rev.* **1964**, *133*, A895.